INSTITUTE OF PHYSICS PUBLISHING JOURNAL OF PHYSICS B: ATOMIC, MOLECULAR AND OPTICAL PHYSICS

J. Phys. B: At. Mol. Opt. Phys. **34** (2001) 2667–2677 www.iop.org/Journals/jb PII: S0953-4075(01)22104-X

Electron-impact studies of atomic oxygen: II. Emission cross section measurements of the O I $^3S^o \rightarrow {}^3P$ transition (130.4 nm)

C Noren, I Kanik, P V Johnson, P McCartney, G K James and J M Ajello

Jet Propulsion Laboratory, California Institute of Technology, 4800 Oak Grove Dr., Pasadena, CA 91109, USA

Received 19 February 2001, in final form 23 April 2001

Abstract

The optical excitation function of the O I $^3S^o \rightarrow {}^3P$ transition (130.4 nm), produced by electron-impact excitation of atomic oxygen, has been measured over an extended energy range from threshold to 1.0 keV. Measurements were obtained in a crossed-beam experiment using both magnetically confined and electrostatically focused electrons in collision with atomic oxygen produced by a microwave discharge source. A 0.2 m vacuum ultraviolet monochromator system was used to measure the emitted O I radiation at 130.4 nm. The relative O I (130.4 nm) emission intensity corresponding to the $^3S^o \rightarrow {}^3P$ transition was then put on the absolute scale by normalization to the O I (130.4 nm) cross section produced by dissociative excitation of O_2 at 30 eV (Kanik *et al* 2000).

1. Introduction

In the preceding companion paper, Kanik *et al* (2001), hereafter referred to as paper I, results were presented concerning the experimental and theoretical electron-impact-induced differential and integral excitation cross sections of atomic oxygen corresponding to the $2s^22p^4\ ^3P \rightarrow 3s\ ^3S^o$ (at 130.4 nm), $2s^22p^4\ ^3P \rightarrow 3d\ ^3D$ (at 102.7 nm), $2s^22p^4\ ^3P \rightarrow 3s'\ ^3D$ (at 98.9 nm), and $2s^22p^4\ ^3P \rightarrow 3s''\ ^3P$ (at 87.8 nm) transitions measured at impact energies of 30, 50 and 100 eV. A general introduction and a survey of the previous investigations on atomic oxygen, both experimental and theoretical, were given in paper I and will not be repeated here.

In this paper, we report electron-impact-induced emission cross sections of the O I $^3S^o \rightarrow {}^3P$ transition at 130.4 nm. The present investigation generates complementary information to the electron-impact direct-excitation cross section work concerning the O I $^3P \rightarrow {}^3S^o$ feature at 130.4 nm (9.51 eV electron energy-loss) reported in paper I. The electron-impact cross sections given in paper I provide information about the direct excitation of the 130.4 nm feature while the present electron-impact-induced emission cross sections provide information about the excitation of the 130.4 nm feature through both direct excitation and cascade from higher-lying excited levels. A comparison of the two, therefore, allows one to estimate the cascade cross section as demonstrated before by our group (Ratliff *et al* 1991, Ciocca *et al* 1997).

0953-4075/01/132667+11$30.00

The O I $^3S^o \rightarrow {}^3P$ transition at 130.4 nm is the most prominent atomic oxygen emission feature in the far ultraviolet (FUV) spectral region and, therefore, is of great interest to aeronomy and astrophysics. However, the shape and magnitude of the experimental excitation function (cross section as a function of impact energy) have remained uncertain and, in fact, controversial. The Link *et al* (1988a, b) reanalysis of airglow/auroral data, based on satellite and rocket measurements of the O I and N_2 LBH (Lyman–Birge–Hopfield) dayglows, led to the conclusion that the cascade contribution to the 130.4 nm emission cross section is much less than the factor of 2 predicted by the optically thick model of Julienne and Davis (1976). This result is further supported by the laboratory measurement of the 130.4 nm emission cross section published by Zipf and Erdman (1985) which included any prompt cascade from higher-lying states. However, on the basis of the same rocket data, using different total electron energy-loss cross sections to calculate the photoelectron fluxes exciting the emissions, Morrison and Meier (1988) suggested a 30% cascade contribution. The situation was further complicated by the results of Cotton *et al* (1993), who also concluded that a substantial (30%) cascade contribution was necessary to explain their rocket measurements. This was done using the Link *et al* (1988a, b) models to interpret their airglow data, but with use of a different solar EUV (extreme ultraviolet) irradiance model in their analysis.

Substantial discrepancies exist between the O I (130.4 nm) emission cross sections found in the literature. For example, the measurements of the O I (130.4 nm) emission cross sections published by Wang and McConkey (1992) differ both in shape and magnitude (lower by 30% at the respective peaks) from the measurements of Zipf and Erdman (1985). Clearly, the differences in the interpretation of FUV airglow data will persist until agreement can be reached on the appropriate cross sections and solar EUV fluxes. Until such time, these differences will continue to manifest themselves in the derivation of thermospheric abundances (Link *et al* 1988b).

In this paper we report the optical excitation function of the O I $^3S^o \rightarrow {}^3P$ transition (130.4 nm) produced by the electron-impact excitation of atomic oxygen over the extended energy range from threshold to 1.0 keV. In presenting our results, we will make comparisons between the present data and those of earlier investigations.

2. Experimental procedures

Electron-impact-induced emission cross section measurements were carried out in our atomic oxygen apparatus, which is shown in figure 1. The apparatus consists of an electron-impact collision chamber, an atomic oxygen source, an electron gun, two pairs of Helmholtz coils and a 0.2 m UV spectrometer equipped with two exit ports where two separate detectors were positioned and employed depending on the spectral region studied. A CsI-coated channeltron electron multiplier (CEM) was positioned on one port and employed for the 40–180 nm wavelength region (FUV), while a photomultiplier tube (PMT) was placed on the second port and used for the 120–300 nm wavelength region (EUV).

Two different electron guns were used in the present experiments to produce the required electron beam: (1) a three-element gun which uses magnetic-field confinement (hereafter referred to as the 'magnetic gun') and (2) a three-element electrostatic gun. The use of these two guns was essential to the success of the present investigation. At low energies ($\lesssim$30 eV), electron beams tend to 'blow up', due to space charge, making it difficult to maintain a reasonably collimated beam at high-electron currents. Thus, the magnetic gun was employed in the low-energy regime ($\leqslant$30 eV). The magnetic gun made use of two solenoids to produce a magnetic field that confined and collimated the electron beam. At higher energies, the confining magnetic field of the magnetic gun tends to trap low-energy secondary electrons that

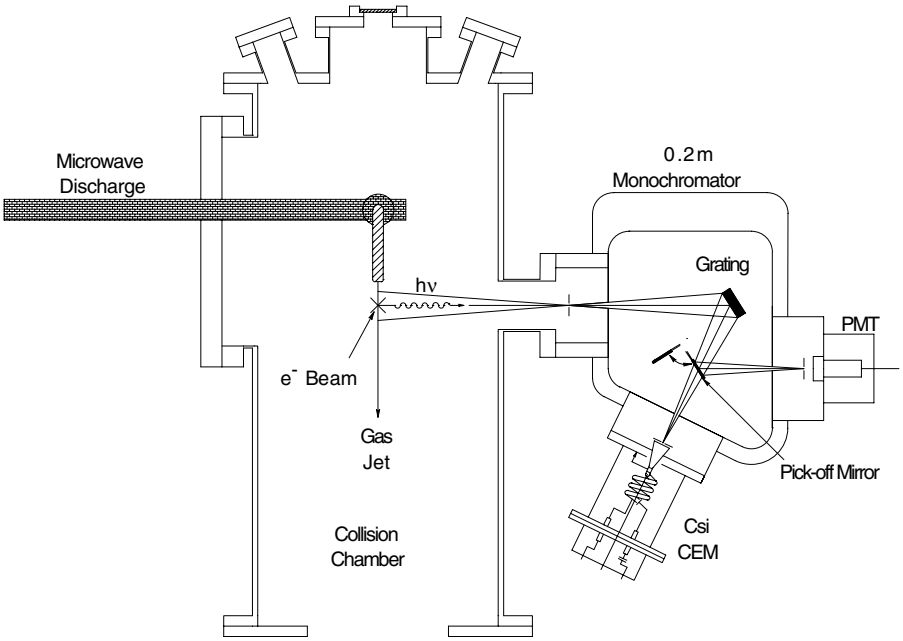

Figure 1. Schematic diagram of the experimental apparatus.

are unavoidably produced by collisions with the gun apertures and through ionization processes. The trapping of these secondary electrons by the collimating magnetic field makes it essentially impossible to obtain an accurate optical excitation function at high energies. Therefore, the electrostatic gun, which is free of these problems, was employed for the measurements in the higher-energy regime ($\geqslant$30 eV).

A detailed description of the magnetic gun/Faraday cup system, as well as the spectrometer system, have been published elsewhere (Ajello *et al* 1988) and will not be presented here. The electrostatic gun uses a standard 2% thoriated tungsten hairpin filament to produce thermionically emitted electrons. Electrons are then extracted by a Pierce and extractor electrode combination and focused into the interaction region by a three-element electrostatic lens. In order to operate the electrostatic gun, it is necessary to eliminate any stray magnetic fields capable of deflecting the electron beam (primarily the Earth's). Therefore, two sets of Helmholtz coils were used to cancel out any magnetic-field components perpendicular to the electron beam axis. When using the electrostatic gun, a modified Faraday cup was used which included an additional metal plate around its opening so that any stray electrons could also be monitored.

Neutral oxygen atoms were created by dissociating molecular oxygen from a 90% O_2 and a 10% N_2 (buffer gas) mixture in an extended air-cooled microwave cavity and were introduced into the collision region. The production of N from the dissociation of N_2 in the discharge source was not appreciable as indicated by our inability to detect any evidence of atomic nitrogen in the target beam. The atomic oxygen source employed in the present investigation is basically identical to that employed in the experiments described in paper I. A similar source was described originally by Murphy and Brophy (1979) and later by Doering and co-workers (Doering *et al* 1985a, b, Gulcicek and Doering 1988).

The electron beam, produced by either the magnetic or electrostatic gun, is crossed at right angles with the target oxygen beam, which effuses from the quartz gas transport tube.

The target oxygen beam contains atomic and molecular components when the discharge is on and is purely molecular when the discharge is off. The emitted photons, corresponding to the radiative decay of collisionally excited states of atomic and molecular oxygen, are then collected by the UV spectrometer at 90° with respect to the electron beam. Care is taken to prevent light contamination from the discharge region. To this end, the quartz transport tube is bent through 90° after leaving the microwave cavity so that a large portion of the photons produced in the discharge region is either scattered away from the detector or absorbed by the tube wall.

In order to analyse the photon signal, it was necessary to determine the percentage of O_2 molecules that were dissociated in the source and remained dissociated at the interaction region (i.e. the dissociation fraction). The dissociation fraction was established by tuning our spectrometer to the centre of the second negative band system of O_2^+ where no atomic oxygen features are present (i.e. in the 234.0–240.0 nm spectral region). Emission signals were then measured with the PMT in both the discharge ON and OFF modes while maintaining a constant oxygen source driving pressure and electron beam current. Since the emission rate of the second negative band of O_2^+, produced by electron-impact-induced ionization of O_2, is directly proportional to the O_2 number density in the target, the dissociation fraction, D, is then related to these two signals, $S^{\mathrm{on}}_{O_2^+}$ and $S^{\mathrm{off}}_{O_2^+}$, by the relationship

$$D = 1 - \frac{S^{\mathrm{on}}_{O_2^+}}{S^{\mathrm{off}}_{O_2^+}}. \tag{1}$$

Here, the effective kinetic temperatures in the gas beam with the discharge on and off are assumed to be the same (Donaldson *et al* 1972). The dissociation fraction was measured before and after each experimental run to ensure consistency.

When measuring the O I (130.4 nm) signal from our target gas jet, a complication arises due to the presence of 130.4 nm radiation being emitted from the electron-impact-induced dissociative excitation of O_2. In this process, electron–molecule collisions cause O_2 molecules to dissociate into excited O atoms, which then decay to the ground state releasing 130.4 nm photons. Therefore, the net discharge ON 130.4 nm emission signal, $S^{\mathrm{on}}_{O+O_2}$, is the sum of the atomic O signal, S^{on}_{O}, and that due to the dissociative excitation of O_2, $S^{\mathrm{on}}_{O_2}$. However, by measuring the 130.4 nm signal with the discharge OFF, $S^{\mathrm{off}}_{O_2}$, at the same source pressure and electron beam current, one can separate the atomic O signal as follows:

$$S^{\mathrm{on}}_{O} = S^{\mathrm{on}}_{O+O_2} - (1 - D)S^{\mathrm{off}}_{O_2}, \tag{2}$$

where we make use of the previously determined dissociation fraction to replace $S^{\mathrm{on}}_{O_2}$ with $(1 - D)S^{\mathrm{off}}_{O_2}$.

The measurements of O I (130.4 nm) emission cross sections were performed in two stages as follows. First the magnetic gun was installed in the system. A research grade gas mixture containing 10% N_2 and 90% O_2 was introduced into the scattering chamber via our discharge source and the dissociation fraction was established as described previously (equation (1)). The integrated intensity of the 130.4 nm spectral feature was then measured from threshold to 30 eV for both discharge ON and OFF conditions. When measuring the low-energy region of the excitation function, the emission signal was collected as a function of impact energy while the impact energy was repeatedly ramped from 0 to 30 eV in steps of 1 eV. Since the electron-beam current could vary substantially as the impact energy was ramped through the measured energy range, a computer was used to monitor the electron current, as measured on the Faraday cup so that the emission signal was collected as a function of integrated electron current. This removed any effects that the energy-dependent electron current variations would have on our measured signal counts. This technique had the added benefit of removing any

variations in the electron current at a given energy that were time dependent. During these investigations, a slow fluctuation in the source gas pressure of the order of 1% was observed. Therefore, the integrated current required to signal a channel/energy advance was set so that the time required for each individual ramp was small (approximately 1 min) compared to the timescale of any gas source pressure fluctuations. Hence any effects of the pressure fluctuations were minimized.

After the low-energy data was accumulated, the electrostatic gun was installed in the collision chamber in order to measure the 30–1000 eV impact-energy range. In this energy regime, the data were collected in impact energy intervals ranging from 20 to 400 eV with the discharge in both the ON and OFF modes. Since the gun performance varied greatly over this energy range, data were collected at each impact energy, on a point by point basis. This allowed for manual re-tuning of the gun at each measured energy. Once again, the data were collected as a function of the integrated electron current so that the individually measured data points could be combined to give a relative integrated signal intensity over the measured energy range.

After subtraction of a flat line dark count (i.e. background), the net emission signal of the 130.4 nm line, at each energy, was then separated into its atomic and molecular components by way of equation (2). This process resulted in two relative excitation functions in the low- and high-energy regimes, respectively.

3. Data analysis

The electron-impact emission cross section, $\sigma(E_0)$, at a given electron-impact energy, E_0, for a particular spectral line of a target species can be expressed as

$$\sigma(E_0) = \frac{KS(1 - p/3)}{\xi\gamma P I_e}\frac{1}{T}, \tag{3}$$

where S is the signal, K is a constant related to the geometry of the detector, γ is the sensitivity of the detector, ξ is the instrumental polarization sensitivity of the system, p is the polarization of the emitted radiation, P is the gas pressure at the entrance to the nozzle under the molecular flow condition, T is the trapping factor, and I_e is the electron current. The trapping of resonance radiation can reduce the emission rate significantly at high gas pressures. The trapping factor, T, for a resonance transition can be determined from measurements of the line intensity as a function of gas pressure. In this paper, the background gas pressure was maintained at approximately 2×10^{-6} Torr in order to ensure that this effect was not significant. Furthermore, the effect of instrumental polarization in the spectrometer and detector systems has been removed (i.e. $\xi = 1$) by rotating the spectrometer such that the plane, defined by the entrance slit and optic axis, is at 45° to the electron beam axis (Clout and Heddle 1969, Donaldson *et al* 1972).

For an ideal gas, the pressure is directly proportional to the density, n. Therefore, if one assumes a constant temperature along with constant electron beam current, equation (3) can be simplified to

$$\sigma(E_0) = \frac{CS(1 - p/3)}{n}, \tag{4}$$

where all of the relevant unvarying factors have been absorbed into a single constant, C. In general, the polarization correction factor (p) is dependent on electron energy. However, in the case of the O I (130.4 nm) line, the polarization is zero. The excited O I 3s $^3S^o$ state is spherically symmetric and, hence, radiation resulting from its decay is unpolarized. Therefore,

in the present case of O I (130.4 nm) emission, equation (4) reduces to

$$\sigma^{130.4} = \frac{CS}{n}. \tag{5}$$

The emission signal intensity, or relative cross section ($S_{\mathrm{O}}^{\mathrm{on}}$) corresponding to radiative decay of the collisionally excited O I $^3\mathrm{S}^{\mathrm{o}}$ state at 130.4 nm, was determined as outlined earlier and then put onto an absolute scale. Normalization of our experimental data was performed by comparing the O I (130.4 nm) signal intensity to the cross section for producing the 130.4 nm photons through electron-impact dissociative excitation of O_2 at 30 eV as measured recently by Kanik *et al* (2000). The normalization procedure is straightforward since the 130.4 nm signal from electron-impact dissociative excitation of O_2 ($S_{\mathrm{O}_2}^{\mathrm{off}}$) was measured under the same experimental conditions (i.e. pressure, electron current, detector orientation) as the O I (130.4 nm) signal ($S_{\mathrm{O}}^{\mathrm{on}}$; see equation (2)). The absolute cross section for producing 130.4 nm emission from electron impact on O is then obtained using the following equation:

$$\sigma_{\mathrm{O}}^{130.4} = \frac{n_{\mathrm{O}_2}^{\mathrm{off}}}{n_{\mathrm{O}}^{\mathrm{on}}} \frac{S_{\mathrm{O}}^{\mathrm{on}}}{S_{\mathrm{O}_2}^{\mathrm{off}}} \sigma_{\mathrm{O}_2}^{130.4}, \tag{6}$$

where $S_{\mathrm{O}}^{\mathrm{on}}$ is determined using equation (2) and $n_{\mathrm{O}}^{\mathrm{on}}$ and $n_{\mathrm{O}_2}^{\mathrm{off}}$ are the number densities of O and O_2 with the discharge ON and OFF, respectively.

The ratio of densities found in equation (6) can be determined in direct analogy with the rate flow analysis outlined in the appendix of paper I. Making identical assumptions regarding dissociation products, thermal equilibrium, and Boltzmann velocity distributions, one can easily show that the number density ratio of equation (6) can be written in terms of the dissociation fraction as

$$\frac{n_{\mathrm{O}_2}^{\mathrm{off}}}{n_{\mathrm{O}}^{\mathrm{on}}} = \frac{1}{\sqrt{2}D}. \tag{7}$$

Combining equations (6) and (7) then yields

$$\sigma_{\mathrm{O}}^{130.4} = \frac{S_{\mathrm{O}}^{\mathrm{on}}}{\sqrt{2}DS_{\mathrm{O}_2}^{\mathrm{off}}} \sigma_{\mathrm{O}_2}^{130.4}. \tag{8}$$

The two data sets (i.e. high and low energy) were normalized to each other at 30 eV in order to give a relative excitation function for the O I (130.4 nm) line from threshold to 1000 eV. Finally, this relative excitation function was put on an absolute scale by normalizing to the 30 eV $\sigma_{\mathrm{O}_2}^{130.4}$ value of 2.06×10^{-18} cm^2 ($\pm 22\%$) given by Kanik *et al* (2000) via equation (8).

4. Results

The results of our absolute electron-impact emission cross section measurements of the O I $^3\mathrm{S}^{\mathrm{o}} \rightarrow {}^3\mathrm{P}$ (130.4 nm) transition are tabulated in table 1 along with the associated experimental uncertainties. A comprehensive review of uncertainties associated with electron-impact emission cross sections involving discharge sources has been given by James *et al* (1997). We, therefore, only discuss details relevant to the estimation of the experimental uncertainties in the current data. It should be pointed out that due to the finite width of the electron beam energy distribution ($\sim$0.5 eV full width at half maximum), we measured a small yet non-zero cross section (0.7×10^{-18} cm^2) at the theoretical threshold energy ($\sim$9.5 eV) as seen in table 1.

It should be noted that, in the present analysis, we assume that two neutral O atoms are produced for every O_2 molecule that remains dissociated at the interaction region (see the

Table 1. Electron-impact-induced emission cross sections for the O I $^3S^o \rightarrow {}^3P$ (130.4 nm) transition.

Energy (eV)	Cross section (10^{-18} cm^2)
9.5	0.7 ± 0.2
10.5	1.7 ± 5.6
11.5	6.1 ± 2.0
12.5	10.5 ± 3.5
13.5	12.7 ± 4.2
14.5	13.5 ± 4.5
15.5	14.1 ± 4.7
16.5	14.5 ± 4.8
18.5	14.9 ± 4.9
20.5	15.0 ± 4.9
22.5	14.8 ± 4.9
24.5	14.6 ± 4.8
26.5	14.4 ± 4.8
30	13.9 ± 4.6
50	10.5 ± 3.6
100	8.3 ± 2.8
200	4.4 ± 1.5
400	3.2 ± 1.1
800	1.7 ± 0.6
1000	1.4 ± 0.5

appendix of paper I). It is conceivable that either oxygen ions and/or metastable oxygen atoms (O I (^{1}D) and O I (^{1}S) at 2.0 and 4.2 eV above the ground state, respectively) could also be created in the discharge source. In both paper I and Doering *et al* (1985a), where similar discharge sources were employed, studies of gas beam composition found no evidence of either oxygen ions or metastable oxygen atoms (1.5% of the atomic O component was given as the upper limit of metastable production in both cases). Likewise, no evidence of such unwanted dissociation products was detected in this paper. Therefore, our assumption is deemed valid.

The main source of experimental uncertainty in the current investigations was introduced during the determination of the dissociation fraction. Unlike the electron energy-loss experiments described in paper I, the dissociation fraction could only be measured at the beginning and end of an experimental run. Since data acquisition times were of the order of 24 h (or more), the discharge conditions were subject to 'drifting'. The dissociation fraction is very sensitive to the tuning of the microwave discharge, which is dependent on both the size and shape of the resonant cavity. The temperature of the cavity can fluctuate slowly over time, causing variations in the size of the cavity, which, in turn, affects the tuning of the cavity. The measured dissociation fractions from several different experimental runs were analysed and in a worst case scenario, a potential drift of up to $\pm 20\%$ was deemed possible. In addition, statistical uncertainties of the order of 10% in the measured $S^{\mathrm{on}}_{O_2^+}$ and $S^{\mathrm{off}}_{O_2^+}$ signals, used in determining the dissociation fraction, contributed to the overall uncertainty. The combination of these uncertainties translated into an overall contribution of about 25% to uncertainty in the final absolute cross section values. It should be noted that the 'drifting' of the dissociation fraction discussed above took place over extended periods of time. As such, the dissociation fraction could easily be considered constant on the timescale of a scan (or even a number of scans) across the measured impact-energy range. Therefore, such 'drifting' had no effect on the relative shape of the excitation function.

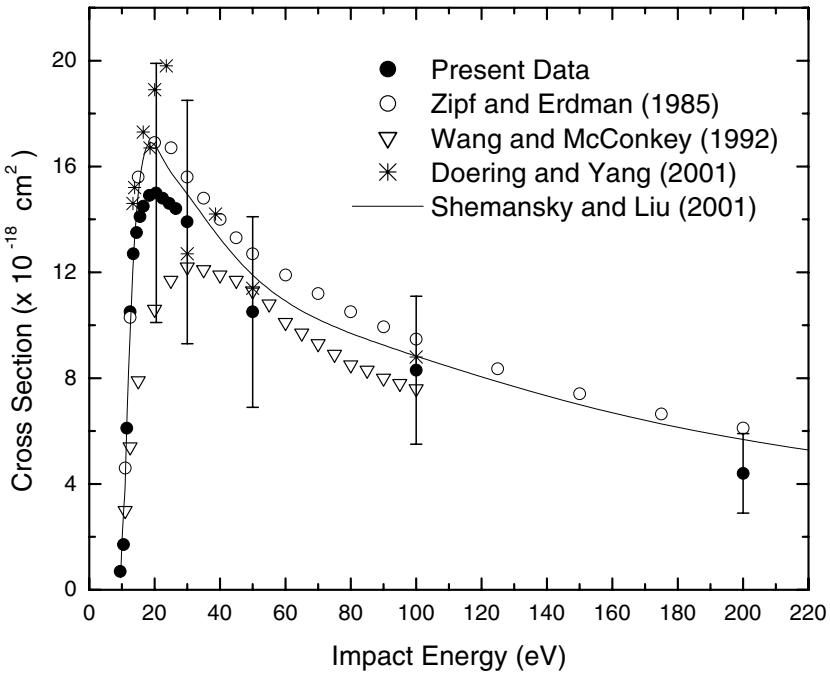

Figure 2. Emission cross sections of the O I $^3S^o \rightarrow {}^3P$ transition (130.4 nm) resulting from electron impact on atomic oxygen at impact energies between the threshold and 200 eV. The results of Zipf and Erdman (1985), Wang and McConkey (1992) and Doering and Yang (2001) have been included for comparison along with the theoretical model of Shemansky and Liu (2001).

The statistical error for the data points varied from $\pm 4.5\%$ near threshold to $\pm 1.4\%$ at 30 eV for the magnetic gun. The statistical error for the electrostatic gun ranged from $\pm 2.2\%$ at 30 eV to $\pm 13.4\%$ at 1000 eV. The total error for each data point was found by adding individual errors in quadrature according to standard error propagation techniques.

5. Discussion

The current absolute excitation function is plotted in figure 2 from 0 to 200 eV alongside the results of previous investigations for comparison. Included in the figure are the data of Zipf and Erdman (1985), Wang and McConkey (1992) and Doering and Yang (2001). In addition, a theoretical model of the excitation function, calculated by Shemansky and Liu (2001), has also been included. The current measurements provide the first experimentally determined cross sections above 200 eV. Therefore, the higher-energy values have been left out of figure 2 in order to facilitate comparisons in the region of overlap.

Despite the somewhat large error bars, the data show a smooth excitation function with almost no scatter. This can be taken to be a sign of reliability in the relative shape of the curve. This coincides with the fact that the largest contributor, by far, to the total uncertainty was the uncertainty associated with the determination of the dissociation fraction. This contribution was manifest only in the calibration to the absolute scale and had no effect on the relative shape of the excitation function. As such, the relative accuracy of the excitation function is considerably better than what a 'first-glance' evaluation of figure 2 might imply. The figure shows that the excitation function rises rapidly from the threshold (9.51 eV) to a maximum

value of 15.0×10^{-18} cm^2 at about 21 eV. It then decreases to 8.3×10^{-18} cm^2 at 100 eV and falls off smoothly with increasing impact energy. At 1 keV, as seen in table 1, the cross section value has fallen approximately an order of magnitude smaller than the peak value.

Although the present results agree, within error bars, with all the available data sets, a few observations can be made. Firstly, the current excitation function peaks at the same impact energy as that of both Zipf and Erdman (1985) and Doering and Yang (2001). In contrast, a substantial discrepancy in the peak position ($\sim$10 eV) is observed when compared with the data of Wang and McConkey (1992), which peaks near 30 eV. Secondly, the shape of our emission function agrees very well with the measurement of Zipf and Erdman (1985). However, the Zipf and Erdman (1985) data are consistently higher by about 2×10^{-18} cm^2 throughout the overlapping energy range (0–200 eV). Finally, the magnitude of our peak lies approximately midway between that of Wang and McConkey (1992) and Zipf and Erdman (1985). It should be noted that the Doering and Yang (2001) data presented here are cascade-corrected direct excitation data. These were obtained by summing the direct excitation cross sections for the 3s ^{3}S^o state (i.e. the 130.4 nm emitting state) plus the direct excitation cross sections for the dominant cascading state, 3p ^{3}P (844.6 nm; see Doering and Yang (2001)). This data set shows some scatter about the peak region but tends to support the excitation function suggested by both this paper and that of Zipf and Erdman (1985). The fact that the cascade corrected data show good agreement with the various emission data indicates that the directly excited 3p ^{3}P level is indeed the dominant cascade contributor to the 3s ^{3}S^o (130.4 nm) state population. This conclusion is particularly clear at 30, 50 and 100 eV impact energies where the 130.4 nm direct excitation cross sections have been well established (see paper I).

It should be pointed out that we have also attempted using NO as a parent gas for atomic oxygen production in our electron energy-loss measurements. The measurements showed strong evidence of O_2 production from the NO based discharge source resulting in further complications in the electron energy-loss spectrum. Given that Wang and McConkey (1992) employed an NO based discharge source in their atomic O emission work, we suggest that the discrepancy between their excitation function and those of others (see figure 2) might be attributed to the presence of O_2 in their beam. Wang and McConkey (1992) assumed that O_2 was not present in their beam. Therefore, if O_2 was in fact present, both the magnitude and shape of their O I (130.4 nm) optical excitation function would have been affected by the inadvertent inclusion of contributions from the O I (130.4 nm) emission from the electron-impact dissociative excitation of O_2. Furthermore, the presence of O_2 in their beam would mean that the assumption of a 1:1 ratio of NO:O, pivotal to their normalization, was incorrect.

Model calculations by Shemansky and Liu (2001) of emission cross sections for the O I ^{3}S^o $\rightarrow$ ^{3}P transition are shown in figure 2. This model has been calculated on the basis of a modified Born approximation constrained by the known dipole absorption oscillator strength and the values of the direct excitation cross section obtained in the experiments of paper I and Doering and Yang (2001) at 50 and 100 eV. Shemansky and Liu (2001) indicate that the cross section model is not definitive because the combined constraints imply very large coupling effects reaching to the 100 eV level. Shemansky and Liu (2001) claim that the calculated excitation cross section is accurate to $\pm$7% between 120 and 1000 eV. Uncertainty below 120 eV is estimated at +25%, $-$5%. The emission cross section calculated by Shemansky and Liu (2001) is based on theoretical cross sections for emission from states cascading into the 3s ^{3}S state. The cascade contributions in the Shemansky and Liu (2001) calculations include the 3p ^{3}P, 4s ^{3}S^o, 3d ^{3}D^o, 4p ^{3}P, 3s ^{3}D^o, 5s ^{3}S^o, 4d ^{3}D^o, 5p ^{3}P, 6s ^{3}S^o, 5d ^{3}D^o, 6p ^{3}P^o, 7s ^{3}S^o and 6d ^{3}D^o states. As seen in figure 2, the model essentially falls between the present excitation function and

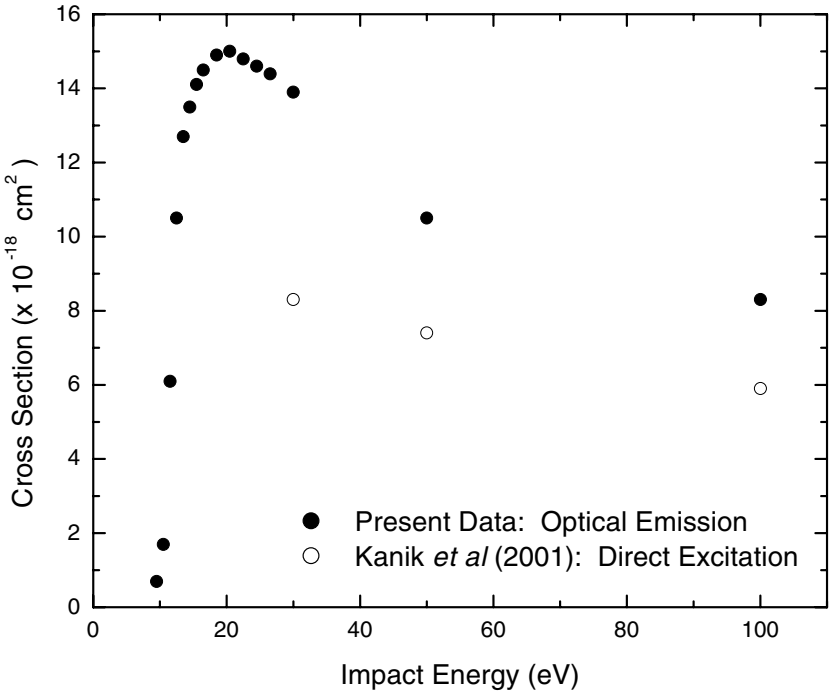

Figure 3. The electron-impact-induced emission cross sections of the O I $^3S^o \rightarrow {}^3P$ transition (130.4 nm) are plotted alongside the direct electron-impact integral excitation cross sections for the O I $^3P \rightarrow {}^3S^o$ transition of Kanik *et al* (2001). Error bars are not shown in the figure in order to avoid clutter. Uncertainties in the present data can be found in table 1, while those in the direct excitation results are quoted as 29% at 30 and 50 eV and 25% at 100 eV.

that of Zipf and Erdman (1985), with the model showing some preference toward the latter.

A useful comparison can also be made with the atomic O direct excitation studies of the preceding companion paper (paper I). Figure 3 shows the emission cross sections of this paper alongside the integral cross section results for the direct excitation of the O I $^3P \rightarrow {}^3S^o$ transition given in paper I.

Electron energy-loss experiments, such as those presented in paper I, give information about the direct excitation of the atomic energy level in question. In contrast, the emission cross sections of this paper arise from populating the 130.4 nm level both by direct excitation as well as through cascade from the higher-lying levels. In the absence of branching to lower-excited states, the direct excitation cross section values must fall below the emission cross section values if, in fact, the cascade contributions are non-negligible. This indeed represents the present situation. As figure 3 shows, the direct excitation values presented in paper I are significantly lower than the corresponding emission values of this paper. Specifically, the comparison suggests a cascade contribution to the emission cross section of approximately 40% at 30 eV and 30% at 50 and 100 eV. This is consistent with the determinations made by Morrision and Meier (1988) and Cotton *et al* (1993) who concluded that a cascade contribution of the order of 30% was necessary to explain their rocket measurements as discussed in the introduction.

6. Conclusions

The agreement between the present excitation function and that of Zipf and Erdman (1985), as well as the model of Shemansky and Liu (2001), in both shape and magnitude, leads to the conclusion that the O I (130.4 nm) excitation function can be considered reasonably well established. This conclusion is further supported by the excitation function given by Doering and Yang (2001) which was determined through a combination of direct excitation measurements.

The present results, in conjunction with the direct excitation cross sections for the O I $^3P \rightarrow {}^3S^o$ transition of Kanik *et al* (2001: paper I), indicate that the cascade contribution to the emission cross section is of the order of 30–40% in the 30–100 eV impact-energy range. This is consistent with the determinations of Morrision and Meier (1988) and Cotton *et al* (1993). We plan to verify these conclusions by performing direct measurements of the cascade contribution to the O I (130.4 nm) emission cross section in the near future.

Acknowledgments

The research described in this paper was carried out at the Jet Propulsion Laboratory, California Institute of Technology, and was supported by the NASA Astrophysics and Planetary Atmospheres Program Offices. Two authors (PVJ and PM) gratefully acknowledge financial support from the Research Associateship Program of the National Research Council. The authors would also like to thank D E Shemansky and X Liu for making the results of their model available prior to publication.

References

Ajello J M *et al* 1988 *Appl. Opt.* **27** 890
Ciocca M, Kanik I and Ajello J M 1997 *Phys. Rev.* A **55** 3447
Clout P N and Heddle W O 1969 *J. Opt. Soc. Am.* **59** 715
Cotton D M, Chakrabarti S and Gladstone G R 1993 *J. Geophys. Res.* **98** 21643
Doering J P, Gulcicek E E and Vaughan S O 1985a *Chem. Phys. Lett.* **114** 334
——1985b *J. Geophys. Res.* **90** 5279
Doering J P and Yang J 2001 *J. Geophys. Res.* **106** 203
Donaldson F G, Hender M A and McConkey J W 1972 *J. Phys. B: At. Mol. Phys.* **5** 1192
Gulcicek E E and Doering J P 1988 *J. Geophys. Res.* **93** 5879
Gulcicek E E, Doering J P and Vaughan S O 1988 *J. Geophys. Res.* **93** 5885
James G K, Slevin J A, Shemansky D E, McConkey J W, Bray I, Dziczek D, Kanik I and Ajello J M 1997 *Phys. Rev.* A **55** 1069
Julienne P S and Davis J 1976 *J. Geophys. Res.* **81** 1397
Kanik I, Johnson P V, Das M B, Khakoo M A and Tayal S S 2001 *J. Phys. B: At. Mol. Opt. Phys.* **34** 2647
Kanik I, Noren C, Makarov O, Ajello J M and McCartney P 2000 *J. Geophys. Res.* submitted
Link R, Chakrabarti S, Gladstone G R and McConnell J C 1988a *J. Geophys. Res. Space Phys.* **93** 2693
Link R, Gladstone G R, Chakrabarti S and McConnell J C 1988b *J. Geophys. Res.* **93** 14631
Morrison M D and Meier R R 1988 *Planet. Space Sci.* **36** 987
Murphy E J and Brophy J H 1979 *Rev. Sci. Instrum.* **50** 635
Ratliff J M, James G K, Trajmar S, Ajello J M and Schemansky D E 1991 *J. Geophys. Res. Planets* **96** 17559
Shemansky D E, Ajello J M and Hall D T 1985a *Astrophys. J.* **296** 765
Shemansky D E, Ajello J M, Hall D T and Franklin B 1985b *Astrophys. J.* **296** 774
Shemansky D E and Liu X 2001 Private communication
Vaughan S O and Doering J P 1987 *J. Geophys. Res.* **92** 7749
Wang S and McConkey J W 1992 *J. Phys. B: At. Mol. Opt. Phys.* **25** 5461
Zipf E C and Erdman P W 1985 *J. Geophys. Res.* **90** 11087